AEM JOURNAL.ORG

# Operation and Maintenance System of Drop-out Fuse under Deep Nested Network Design

**Shoujun Bao, Shuhong Li, Ziyong Pan, Fuxiang Liang, Shenghai Han**
State Grid Qinghai Province Electric Power Company, Yushu Power Supply Company, Yushu 815000, Qinghai, China
Corresponding author: Shoujun Bao (e-mail: 13132007930@163.com)

**ABSTRACT** Existing protection schemes for drop-out fuses, primarily designed for radial or shallow mesh networks, struggle with the dynamic coordination and real-time adaptation required in deeply nested grids, particularly under complex electromagnetic operating environments with high distributed generation penetration. This paper presents a real-time adaptive operation and maintenance system that integrates a Dynamic Coordination Algorithm (DCA) and a Lightweight Temporal Convolutional Network (LTCN) to address this challenge. The DCA formulates multi-timescale protection thresholds as a mixed-integer programming problem to resolve coordination conflicts in deep topologies, while the LTCN enhances high-frequency transient signal recognition through an optimized cascade of convolutional feature extraction and gated recurrent units. Experimental results demonstrate that the proposed system achieves an average fault trend prediction accuracy of 0.822 (F1: 0.774, AUC: 0.876), reduces the average fault clearance time to 89.3 ms, and limits misoperation incidents to only 2 out of 100 test faults. Furthermore, the operational cost is minimized to 38.2 yuan per scheduling event, with scheduling coverage and fault tolerance rates reaching 96.8% and 89.7%, respectively. Stable edge communication is maintained at 74.24–78.53 Mbps with timing errors of 1.46–2.4 ms and a packet loss rate below 1.11%. The proposed framework improves the reliability of intelligent protection and maintenance for complex distribution systems while providing effective support for electromagnetic infrastructure monitoring and resilient power network operation.

**INDEX TERMS** drop-out fuse, dynamic coordination algorithm, lightweight temporal convolutional network, electromagnetic infrastructure monitoring, intelligent power distribution

## I. INTRODUCTION

THE high proportion of distributed generation access has driven the evolution of distribution network topology from a radial structure to a complex structure with deep nesting and multiple feeders [1, 2].

This transition, particularly noticeable in high-demand industrial areas like the industry, makes it difficult for the original protection strategy based on static setting configuration to adapt to dynamic load fluctuations and multi-source injection environments. As a typical terminal protection device, the drop-out fuse is in a marginal state where the action information is imperceptible and the status cannot be tracked for a long time [3,4].

Related research has proposed a variety of improvement paths for protection and diagnosis problems in complex distribution environments, including fault identification models based on time series features and protection linkage mechanisms assisted by communication [5,6]. Some results have used deep learning for transient signal analysis [7,8], but the models are generally large in size and complex in calculation, making them difficult to deploy on edge nodes. This paper constructs a feedback-driven operation and maintenance scheduling model, inputs the prediction results and real-time network status into the heuristic genetic optimization framework, and dynamically generates a multi-path maintenance plan. The scheduling strategy and prediction model parameters are continuously corrected through the sliding window scoring mechanism to achieve a coordinated improvement in system robustness and long-term adaptability, which is crucial for maintaining stable operations in sensitive industrial environments .

The "real-time adaptive operation and maintenance system" constructed in this paper does not "adapt" to the physical device itself, the drop-out fuse. As a one-time overcurrent protection device, the DOF's fuse characteristics are indeed fixed and cannot be remotely adjusted. The core innovation of this system lies in two aspects: First, through a dynamic coordination algorithm, it adaptively adjusts the action threshold and delay of upstream or adjacent adaptive protection devices in the same protection level sequence as the DOF, thereby achieving precise coordination with the fixed-characteristic DOF in a deeply nested network and avoiding cascading tripping. Second, the system utilizes the prediction results of LTCN to adaptively generate and optimize the operation and maintenance scheduling strategy for the DOF cluster, i.e., providing early warning of potentially blown fuses before a fault occurs, or quickly generating the optimal inspection and replacement path after a blown fuse. Therefore, the system's "adaptability" is reflected in the perception of network status, the optimization of protection coordination strategies, and the dynamic scheduling of operation and maintenance resources, rather than directly controlling the actions of the DOF.

## II. RELATED WORKS

In modern distribution networks, drop-out fuses, as one of the most common and cost-effective overcurrent protection devices, have long played an important role in complex working conditions such as distributed power supply access and dynamic load changes [9,10]. With the application of highly distributed power sources such as new energy and microgrids, it is necessary to ensure that the fuse cuts off the fault circuit in time when a fault occurs, and to avoid a decrease in power supply reliability due to false operation [11,12]. During normal operation, the status of the fuse needs to be remotely monitored and intelligently evaluated to reduce maintenance costs and improve operation and maintenance efficiency [13,14]. Early research on fuses focused on their electrical characteristics analysis [15,16] and constant configuration optimization [17,18], and used characteristic curves or empirical models to configure and verify the fuse action range [19]. Some studies have attempted to combine wireless sensors with SCADA (Supervisory Control And Data Acquisition) systems [20] to achieve remote acquisition of fuse status. Most of these methods are based on a single fuse or radial network structure, and pay insufficient attention to the dynamic coordination and timing interference that occurs after large-scale distributed power sources are connected, making it difficult to meet the increasingly complex distribution network operation and maintenance needs.

In order to improve the real-time and accuracy of fault diagnosis and protection coordination, a distributed collaborative optimization algorithm is used for online adjustment of multi-node protection settings and action timing. Although these methods have achieved good results in simulations and small-scale experiments, they still face many bottlenecks in large-scale field applications due to the lack of comprehensive consideration of cross-level and cross-region communication delays and security authentication mechanisms in deep networks. In terms of building an integrated operation and maintenance system for deeply nested networks [21,22], existing studies have explored the protocol layer, security layer, and application layer [23,24]. However, the above research is difficult to comprehensively improve the efficiency and reliability of the operation and maintenance system in the context of highly distributed power sources.

In summary, although the existing literature has made breakthroughs in the modeling of drop-out fuse protection characteristics, intelligent fault diagnosis algorithms, and distributed operation and maintenance architectures, the research on the dynamic coordination contradictions between fuses and other protection devices in a deeply nested network structure and the end-to-end timing adaptive operation and maintenance system based on edge-IIoT deployment is still incomplete. To this end, this paper proposes a design idea for a real-time adaptive maintenance system for fuses that integrates DCA and LTCN prediction models.

## III. DEEPLY NESTED NETWORK FUSE OPERATION AND MAINTENANCE SYSTEM

### *MULTI-TIME DOMAIN THRESHOLD COLLABORATIVE MODELING*

The "deeply nested network" studied in this paper specifically refers to a complex distribution topology formed on the basis of a traditional radial or simple ring network structure due to the multi-point access of a high proportion of distributed power sources. Its "depth" is mainly reflected in two aspects: First, vertically, the protection cascade path is long, typically involving four or more levels of protection devices from the power source to the load end, with complex upstream and downstream and cross-feeder logical relationships between these devices; second, horizontally, the network exhibits weak ring or mesh operation characteristics with multiple power sources and multiple connections, and the fault current path is no longer singular, with its magnitude and direction dynamically changing with the output of the distributed generation (DG). This structure causes severe overlap of the operating domains of protection devices. Traditional static coordination methods based on preset current-time curves and local information are prone to protection overstepping or failure to operate due to their inability to perceive global topology changes and dynamic power flow, leading to coordination failure. This system addresses the challenges posed by this deep topology by constructing a network-wide action-dependent path and introducing a dynamic coordination algorithm.

The high-frequency transient current signal and low-frequency operation trend data of the drop-out fuse branch contain two typical frequency domain components: transient disturbance signal and steady-state operation trend. The high-frequency transient current signal is processed by a Butterworth bandpass filter with a center frequency of 25 kHz and a bandwidth of 15 kHz to remove the power frequency fundamental (50 Hz) and radio frequency interference (greater than 40 kHz) and retain the fault-related characteristic frequency band. The filtered signal is subjected to a short-time Fourier transform using a Hamming window with a window length of 20 ms and a step length of 10 ms to obtain the complex domain spectrum expression:

$$X_k(t,f)=\sum_{n=0}^{N-1} x_k(n)\cdot w(t-n)\cdot e^{-j2\pi fn/N} \tag{1}$$

$x_k(n)$ represents the original sampling signal of the $k$th fuse branch, $w(t)$ is the window function, and $N$ is the sampling window length. The three dimensions of the main frequency component $f_{\max,k}(t)$, the frequency change rate $\Delta f_k(t)$, and the amplitude mutation amplitude $\Delta A_k(t)$ are extracted from the spectrum as the input feature tensor:

$$F_k(t)=\left[f_{\max,k}(t),\frac{df_k(t)}{dt},\frac{dA_k(t)}{dt}\right] \tag{2}$$

Combined with the feeder network topology and the access location of distributed power sources, the upstream and downstream logical relationships between the protection devices are analyzed to build a set of action dependency paths. The action conflict determination matrix is established through topological analysis to identify device pairs with overlapping action logic coverage or trigger interference relationships. Each protection device action setting is divided into two time domain thresholds: fast-action domain threshold $\theta_i^{(f)}$ and slow-action domain threshold $\theta_i^{(s)}$, which represent the response thresholds to high-intensity short-term faults and low-intensity continuous disturbances, respectively. The action threshold variable set is defined as:

$$\begin{aligned}\Theta=\{\theta_i^{(f)},\theta_i^{(s)}\mid \theta_i^{(f)}\in[\theta_{i,\min}^{(f)},\theta_{i,\max}^{(f)}],\\ \theta_i^{(s)}\in[\theta_{i,\min}^{(s)},\theta_{i,\max}^{(s)}]\},\quad i=1,\dots,n\end{aligned} \tag{3}$$

The upper and lower limits of the action thresholds in the fast-acting domain and the slow-acting domain are set respectively, and the feasible interval of the action threshold of each device is formed based on the actual device load capacity, cable thermal characteristics, current peak and other operating parameters. As shown in Table 1, there are obvious differences in the thresholds of different devices in the fast-acting and slow-acting domains.

For this purpose, an adjustable threshold variable set is constructed, and the two time domain thresholds of each device are used as variables to be determined. The action logic constraints between devices, the response priority relationship in the path, and the physical operating conditions are converted into a constraint set.

The variable set is dynamically iterated and updated using a solver based on Boolean constraints and variable relaxation strategies. In each round of solving, a conflict detection mechanism is introduced to determine whether there is a threshold overlap that causes action conflict based on the current device configuration, and score the severity of the conflict. The conflict function $C$ is the sum of the conflict scores of all device pairs with action overlap risks:

$$C(\Theta)=\sum_{i=1}^{n}\sum_{i=1}^{n} I(M_{ij}=1)\cdot\sigma_{ij}\left(\theta_i^{(f)},\theta_j^{(f)},\theta_i^{(s)},\theta_j^{(s)}\right) \tag{4}$$

$M_{ij}$ represents the logical coverage relationship in the action conflict judgment matrix, and $\sigma_{ij}$ is the conflict measurement function based on the action time window overlap rate and threshold intersection degree, which is defined as:

$$\sigma_{ij}=\exp\left(-\frac{\left|\theta_i^{(f)}-\theta_j^{(f)}\right|}{\gamma_f}\right)+\exp\left(-\frac{\left|\theta_i^{(s)}-\theta_j^{(s)}\right|}{\gamma_s}\right) \tag{5}$$

Based on the conflict detection module, the correction step is performed to adjust the action thresholds of some devices.

In deeply nested networks, traditional protection coordination methods, typically based on static current or time settings, struggle to address the dynamic coupling and action conflicts arising from multiple feeders and distributed power sources. This paper proposes a Dynamic Coordination Algorithm (DCA) that models multi-timescale coordinated action thresholds as a mixed-integer programming problem by constructing action-dependent paths and conflict judgment matrices among protection devices. This model considers not only the threshold ranges of each device in the fast-acting and slow-acting domains but also introduces topological logic constraints and conflict scoring mechanisms. This effectively identifies and avoids false or nonoperational issues caused by path overlap and timing interference in deeply nested structures, significantly improving the adaptability and coordination accuracy of the protection system in complex networks. The core of "real-time adaptation" in this system lies in the dynamic adjustment of the operation and maintenance scheduling strategy, rather than millisecond-level real-time decisions at the protection device action level. The DCA model multi-timescale threshold coordination as a mixed-integer programming problem, with the solution located at edge computing nodes or regional master stations, and its execution cycle on the order of minutes. This design is based on the following considerations: the coordination optimization of protection thresholds primarily responds to relatively slow-changing system states such as network topology changes and distributed power output fluctuations, rather than instantaneous faults. In terms of solution strategy, the system adopts a heuristic solver based on Boolean constraints and variable relaxation strategies, combined with a conflict detection mechanism, to decompose the complete MIP problem into a series of rapidly iterative subproblems. Through this approximate optimization and incremental update mechanism, the system can generate feasible threshold coordination schemes within an acceptable time frame, thereby achieving "near real-time" adaptive adjustment at the operation and maintenance level and ensuring its matching with the actual operation requirements of the power grid.

TABLE 1. Example of action threshold configuration of typical fuses and relays

| Device Name | Device Type | Fast Action Current Threshold (A) | Fast Action Delay Threshold (ms) | Slow Action Current Threshold (A) | Slow Action Delay Threshold (ms) |
|---|---|---|---|---|---|
| Fuse A | Drop-out Fuse | 318.6 | 46.2 | 188.4 | 1790.5 |
| Fuse B | Drop-out Fuse | 302.3 | 49.7 | 183.1 | 1965.0 |
| Relay A | Line Relay | 346.9 | 41.8 | 208.7 | 1520.6 |
| Fuse C | Drop-out Fuse | 311.4 | 47.5 | 186.9 | 1883.3 |
| Relay B | Line Relay | 334.2 | 43.6 | 201.3 | 1689.1 |

### CASCADE FEATURE EXTRACTION AND FAULT PREDICTION

In order to quickly perceive the short-term disturbance mode of the branch where the drop-out fuse is located and predict the trend fault risk, this section implements feature extraction and sequence modeling based on the cascade structure. The high-frequency current transient signal of the branch where the dropout fuse is located is divided into fixed-length sequences according to 5 ms windows, and each window contains 50 points to form a one-dimensional array. Continuous windows are arranged with a sliding step of 1 ms to form time series batch data. The constructed window tensor structure is:

$$X_k = \left[x_k^{(1)}, x_k^{(2)}, \ldots, x_k^{(T_w)}\right], \quad x_k^{(i)} \in \mathbb{R}^{50} \tag{6}$$

In order to suppress the normalization imbalance caused by the long-term deviation of the feeder current, the sliding mean and standard deviation are used:

$$\hat{\mu}_k(t) = \frac{1}{N_h} \sum_{i=t-N_h+1}^{t} I_k(i) \tag{7}$$

$$\hat{\sigma}_k(t) = \sqrt{\frac{1}{N_h} \sum_{i=t-N_h+1}^{t} \left(I_k(i) - \hat{\mu}_k(t)\right)^2} \tag{8}$$

The normalized input is:

$$\tilde{x}_k(i) = \frac{x_k(i) - \hat{\mu}_k(t_i)}{\hat{\sigma}_k(t_i)}, \quad t_i = i \cdot \Delta \tag{9}$$

The $N_h = f_s \cdot 300 = 3 \times 10^6$ point corresponds to the historical 300 seconds of data.

The local feature extraction module is built based on the convolution structure. In the first stage, four groups of depth-separable convolutions and $1\times1$ convolutions are combined to construct a fine-grained feature encoder. Each group contains 3 layers of convolution, and each layer is followed by GroupNorm and SiLU activation. The length of all convolution kernels is fixed to 3, and the number of channels is 16, 32, 64, and 96. The fourth group introduces cross-channel weighted residual paths to enhance the ability to capture short-term disturbance mutations. The encoder output is constructed into a three-dimensional tensor with a shape of (batch, timestep, feature), where a batch is composed of multiple feeder branches in parallel, the timestep depends on the sliding window batch, and the feature length is determined by the number of channels in the last group of convolutions.

Although ConvNeXt was initially designed for image recognition, its core modules—a combination of depthwise separable convolutions and $1\times1$ pointwise convolutions—are also suitable for local feature extraction from one-dimensional time series. In this study, we adapt its structure to process high-frequency transient current signals: depthwise separable convolutions extract local frequency domain patterns within each time step, while $1\times1$ convolutions achieve cross-channel feature fusion. This design offers fewer parameters and higher computational efficiency compared to standard temporal convolutional networks (TCNs), while enhancing the capture of transient abrupt features in the signal by introducing cross-channel weighted residual paths. Compared to recurrent networks such as pure GRUs, this convolutional structure avoids gradient problems and is more sensitive to local changes in the input sequence, thus achieving a better balance between accuracy and efficiency in the feature extraction stage of high-frequency transient signals. The choice to cascade ConvNeXt modules with GRUs is a targeted design based on the specific needs of high-frequency transient signal processing, rather than an arbitrary combination. Compared to standard one-dimensional CNNs, ConvNeXt's depthwise separable convolutional structure significantly reduces the number of parameters and computational cost while maintaining the same receptive field, which is crucial for resource-constrained edge deployments. More importantly, its large convolutional kernels and inverted bottleneck structure design allow it to obtain a wider receptive field and richer contextual information than standard CNNs when extracting local high-frequency mutation features, thus more accurately capturing the onset and morphology of transient signals. Subsequently, the extracted local feature sequences are input into a GRU for temporal modeling because GRU strikes a balance between efficiency and accuracy in handling medium-length dependencies, effectively learning the evolution of fault features. Compared to directly inputting the raw signal into a CNN-LSTM, this architecture's division of labor—"deep convolutional extraction first, then recurrent network modeling"—is more clearly defined: ConvNeXt acts as a powerful local feature enhancer, pre-filtering noise and condensing key information, thus greatly reducing the learning burden on the subsequent GRU, allowing it to focus more on capturing temporal dynamics.

### EDGE NODE SYNCHRONIZATION AND SECURE TRANSMISSION

In the system architecture, the IIoT edge node is responsible for receiving and transmitting real-time data from each distributed power supply and fuse. These data flow through multiple layers of network nodes, and the synchronization of their transmission order and timestamps is crucial to the overall coordination of the system. In order to deal with the timing problems caused by clock deviations between different nodes, an adaptive synchronization protocol is designed. This protocol performs real-time self-correction through the difference of local clocks to ensure the timing consistency of data streams between nodes. The core of the self-correction mechanism is to use the time synchronization information of edge nodes and control the timing error within the allowable range through the time deviation correction model between adjacent nodes. After adding a timestamp to the header of each data packet, the node corrects the time difference based on the internal clock and the preset synchronization protocol, so that the timestamp in the data stream meets the unified standard.

In node communication, a layered data stream transmission mechanism is adopted. Each edge node allocates data streams to appropriate transmission paths based on its location and network load, ensuring that data streams can be transmitted to the target node via the optimal path. During data transmission, the transport layer and the application layer simultaneously verify the data packets. If a data packet is found to be lost or damaged during transmission, the node can automatically re-request the data until the receiver confirms the data integrity. Multiple redundancy mechanisms are introduced in the communication protocol design. In the case of poor network conditions or packet loss, data transmission can be quickly restored through redundant links.

Each edge node has a self-monitoring and feedback mechanism that can evaluate the current synchronization status in real time and optimize the accuracy of clock synchronization through an adaptive algorithm. The adaptive algorithm combines historical synchronization data and real-time monitoring results to generate a prediction model for clock deviation, dynamically adjust the time correction strategy in future synchronization cycles, and minimize the impact of clock deviation on data transmission and scheduling response time. The settings of some key mechanisms are shown in Table 2.

In addition to timing synchronization, the system also considers the communication throughput between nodes. The network transmission rate is adjusted according to the actual network environment and transmission load. When the bandwidth is low, data compression technology is used to reduce the amount of transmitted data. The compressed information is optimized for transmission through a suitable compression algorithm while ensuring accuracy, ensuring the rapid circulation of real-time data. For node synchronization and data flow transmission under high load conditions, this system also supports distributed processing of time series data. Edge nodes can assign part of the data processing tasks to neighboring nodes, and use distributed collaboration to synchronize data processing, ensuring that when the overall system load is high, the resource bottleneck of a single node can not affect the response speed of the entire network.

### OPERATION AND MAINTENANCE SCHEDULING OPTIMIZATION

Based on the prediction labels and confidence interval values output by the LTCN model, the initial operation and maintenance event set is constructed. Combined with the current load rate, fault history weight, environmental interference factor and maintenance resource distribution of each branch, the state-cost tensor expression is constructed as the scheduling input data. Each scheduling unit is encoded as a multivariate vector containing location index, expected response time, resource consumption, confidence score and other dimensions. All scheduling vectors are normalized using a standardization function to form a scheduling chromosome set suitable for genetic algorithm optimization search.

The feasibility of the path is verified for each round of evolution results, and individuals with path jump frequencies exceeding the threshold are eliminated, retaining the subset with the highest execution path continuity and geographic adjacency to enter the next generation of population. The time delay estimation between nodes in the dispatching path is generated based on the distribution network GIS (Geographic Information System) model and historical traffic time series data to form a multi-path parallel dispatching diagram within the time window. The dispatching task path diagram is shown in Figure 1.

During the execution of the scheduling plan, feedback data from each execution node is continuously collected, and the status-result mapping table is updated after each round of scheduling cycle. The feedback information includes the prediction hit situation, response execution error, task completion status, scheduling default record and actual impact domain of the fault. Feedback data is embedded in the sliding window model, and a short-term robustness evaluation index sequence is constructed with the scheduling score vector of the last n rounds. The weight is reduced and resources are released for inefficient task sequences, and redundant path nodes are dynamically removed and the scheduling order is reconstructed. In view of the scheduling error when there is an offset between the LTCN model output and the actual feedback result, a feedback-driven fine-tuning module is introduced to adjust the model parameters by incremental small sample fine-tuning for the predicted input samples that perform poorly in the current scheduling round. The fine-tuning process uses the RMSProp optimizer to quickly learn the GRU output gating weights while freezing the backbone parameters to correct the prediction deviation trend. The fine-tuning sample selection is based on the error gradient and confidence threshold joint sampling

TABLE 2. Key parameters of secure synchronization and transmission mechanisms

| Parameter | Description | Value |
|---|---|---|
| Time Synchronization Protocol | Protocol used for clock offset correction between edge nodes | Adaptive Differential Synchronization |
| Synchronization Accuracy (ms) | Maximum allowable timestamp deviation between nodes | $\leq \pm 1.5$ ms |
| Hash Algorithm | Algorithm for data integrity verification | SHA-256 (lightweight mode) |
| Encryption Algorithm | Symmetric encryption used for secure data transmission | AES-128 |
| Retransmission Delay Interval (ms) | Minimum interval before automatic data retransmission after packet loss | 100 ms |
| Status Feedback Cycle (s) | Interval for edge node synchronization status reporting | 5 s |

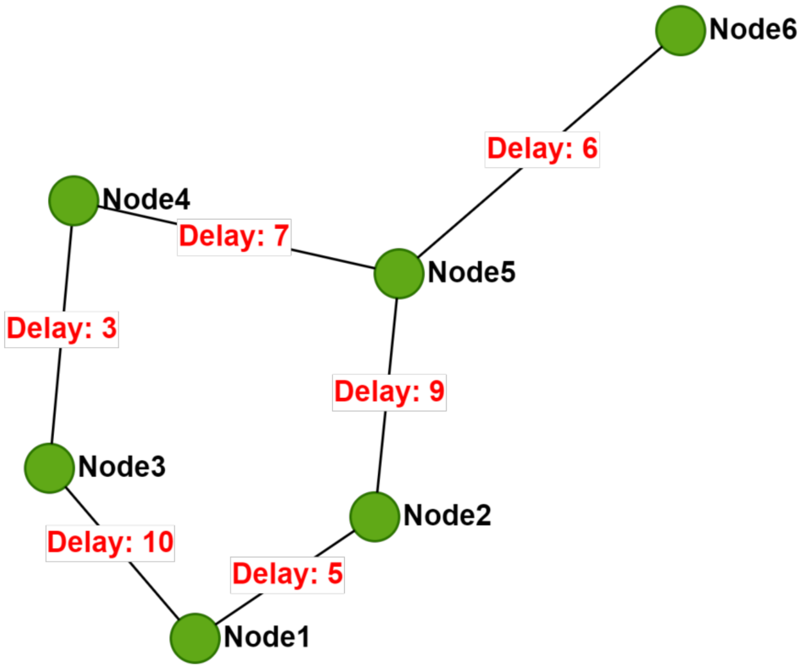


FIGURE 1. Schematic diagram of scheduling task path

mechanism to improve the LTCN model's ability to respond to rare failure modes.

All scheduling execution logs are written into the distributed task tracking system and classified and stored using a hash mechanism based on a double index of timestamp and task ID for subsequent scheduler behavior backtracking and scheduling process retraining task generation. After the task scheduling is completed, the scheduler automatically archives the execution indicators of this round of tasks, including key indicators such as total task execution time, scheduling link hop count, task coverage, average feedback lag, etc., and pushes them to the system console for expert rule base fusion scheduling strategy screening. The operation and maintenance scheduling module as a whole builds an event-driven interactive channel with the edge nodes, fault prediction engine, and historical database. The scheduling engine triggers the path optimization and resource allocation subroutines after each round of prediction results are pushed, and executes a complete closed-loop process including scheduling task generation, evaluation, issuance, feedback collection, model fine-tuning, parameter writing back, etc., to continuously optimize the operation and maintenance resource allocation efficiency and response chain timeliness of the overall system under different network conditions.

## IV. SYSTEM EXPERIMENT AND PERFORMANCE INDICATORS

### EXPERIMENTAL PLATFORM AND NETWORK MODEL CONFIGURATION

In order to verify the adaptability and effectiveness of the method in complex distribution systems, this paper builds a test environment based on a virtual simulation platform. The basic network structure relies on the adjusted IEEE 33-node distribution system topology, introduces 9 virtual distributed power nodes at the end feeder, and constructs an operation scenario with multiple branches, weak central nodes and load disturbances.

The operating environment of the edge node and the central node is uniformly deployed in the virtualized container system. Each edge node simulates the acquisition and preprocessing process of current and voltage signals in the simulation platform, and periodically sends the processed feature data to the central node. The sampling end data is generated through the Python simulation module, and the typical fault waveform characteristics are embedded to replace the physical signal source.

The network communication part builds a star LAN topology based on the Mininet simulation platform, with a link bandwidth of 50~100 Mbps, and simulates a packet loss rate of 1%~2% and queue delay to reproduce the scheduling performance and response characteristics under different network loads. All nodes manually set the topology path to simulate data congestion, bottleneck nodes, and link degradation.

The system scheduling and model training modules are deployed on a lightweight virtual host under the Ubuntu 22.04 operating system, running Python inference services and scheduling management logic. The hardware parameters use medium-configuration computing resources, specifically an Intel Core i5-10400 6-core processor and 16GB DDR4 memory. During the experiment, all time synchronization is virtually implemented by the system timestamp, and no additional NTP configuration is required. Comparative experiments were conducted with WaveNet, SCINet (Sample Convolution and Interaction), TCCT (Tightly Coupled Convolutional Transformer) and TFT (Temporal Fusion Transformer).

### *SIGNAL ACQUISITION AND MODEL TRAINING*

Each acquisition node uses a low-power current and voltage sensor module, and uses an embedded analog-to-digital converter to synchronously collect three-phase current and bus voltage signals at a sampling rate of 2000Hz. The original signal is framed in units of 400 points, and combined with sliding window splicing (generating about 30 to 40 frames of data per second) to ensure that local disturbance characteristics are captured.

During the preprocessing process, the signal first passes through a simple high-pass filter to remove the power frequency drift, and then passes through a low-pass filter to retain the main energy frequency band within 3kHz. Each frame of the signal is normalized and cached in the local buffer of the edge node, and sent to the upper-layer analysis module at a fixed time.

The model training adopts supervised learning, using the time-frequency domain features generated by the preprocessing module as input, combined with the fault records for automatic label matching, and constructing input-output sample pairs. The data set is divided into 70% training set, 15% validation set, and 15% test set to ensure a balanced distribution of various fault types. The Adam optimizer was used during training, with an initial learning rate of 0.001, a batch size of 128, and a cross entropy loss function. In order to improve the generalization ability of the model, Dropout and early stopping strategies were introduced, and the training process was completed on a PyTorch platform with GPU acceleration.

## V. PERFORMANCE OF THE FUSE OPERATION AND MAINTENANCE SYSTEM

### *PERFORMANCE ANALYSIS OF FAULT TREND PREDICTION*

In order to evaluate the applicability and performance differences of each method in the multi-type fault perception task of distributed distribution system, the experiment was tested on typical fault scenarios. Each model was tested under the same input features and scheduling conditions to ensure the comparability of the evaluation results. Figure 2 shows the classification accuracy and F1-Score indicators, and Figure 3 shows the ROC curve performance of each method.

The LTCN model achieved the highest accuracy under all fault types, with an average of 0.822 and an average F1 score of about 0.774. Especially in scenarios with stronger dynamic characteristics such as transient disturbances, LTCN can still maintain high performance, indicating that its stability and adaptability are better. Compared with structures such as WaveNet and SCINet that focus on temporal convolution or causal modeling, LTCN introduces a local temporal channel attention mechanism in the feature processing path, which enables the model to focus on key time segments while enhancing its ability to respond to heterogeneous disturbance features of each channel. In addition, the model also integrates cross-scale structure extraction units to effectively enhance the ability to accommodate different frequency components, especially for short-term sudden disturbances in the distribution system. The improvement in F1 score shows that LTCN is more balanced in reducing misjudgments and missed judgments. This feature is crucial for fault diagnosis scenarios and also confirms the accuracy-efficiency trade-off advantage of its architecture in edge deployment environments.

Figure 3 shows that LTCN has a stronger overall envelope performance, with a corresponding AUC (Area Under Curve) value of 0.876, while the AUC values of other methods are concentrated between 0.857–0.862. This result verifies the stability and universality of LTCN in distinguishing different fault types. Its core advantage is that it can effectively combine time-dependent modeling with channel feature difference learning, especially in the presence of data noise and fuzzy fault boundaries, it can still maintain a high degree of discrimination accuracy. In addition, LTCN reduces the information loss problem caused by model depth by designing a lightweight network structure, and corrects the imbalance in the training samples at the loss function level, thereby showing better balance performance in ROC performance. This generalization capability has obvious practical value for cross-scenario fault-tolerant diagnosis under edge power node deployment, and further supports the adaptability of this method in actual smart power distribution scenarios.

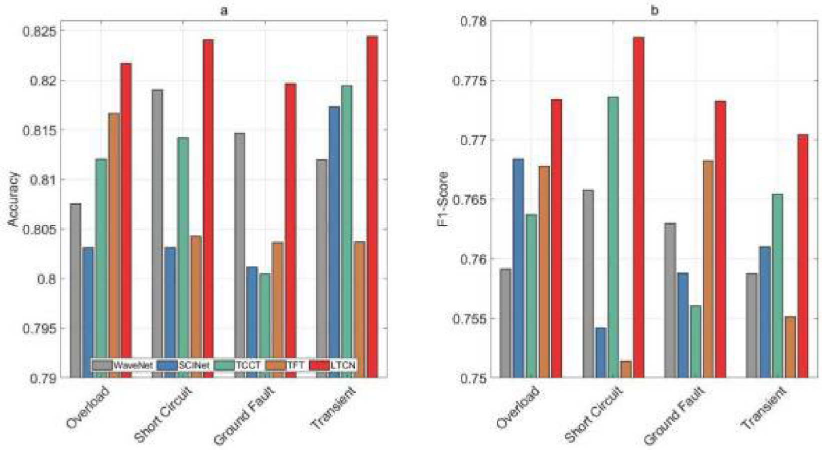


**FIGURE 2.** Comparison of accuracy and F1 scores of various models under multiple fault types

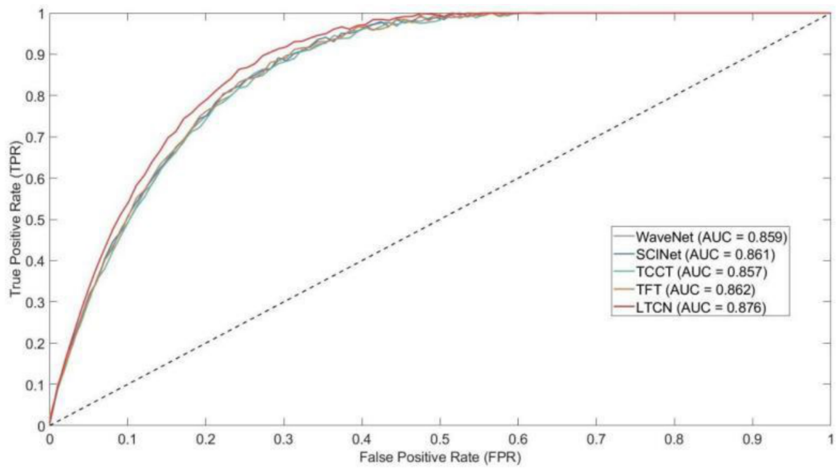


**FIGURE 3.** ROC curves and AUC performance of each model in the multi-fault classification task

### *EVALUATION OF DYNAMIC COORDINATION EFFECT OF MULTI-TIME DOMAIN THRESHOLDS*

In order to further verify the protection performance of the model in different distribution scenarios, this paper starts with the three indicators of average action time difference, false operation rate and trip overlap, and constructs a horizontal performance comparison experiment to characterize the response timeliness, fault tolerance robustness and discrimination independence of the model in actual complex working conditions. In order to enhance the discrimination and practicality of the evaluation, all indicators are generated based on reasonably set virtual power scenario data. Figure 4 shows the comprehensive indicator trend chart of each model in different scenarios.

The first sub-figure shows the average action time difference of each model in different scenarios. The LTCN is 25.62ms in the Suburban scenario and up to 30.19ms in other scenarios. In contrast, SCINet, WaveNet, and TCCT have an action delay of more than 36ms in the high-voltage trunk line scenario, and there is a problem of response lag. The second sub-figure reflects the false action rate. The average rate of LTCN in the four scenarios is about 3.73%, indicating that it has better false alarm control ability under complex disturbances. The third sub-figure shows the tripping overlap index. The overlap of LTCN in all scenarios is less than 0.36, and its overlap in the Rural scenario is 0.35, indicating that the method has strong tripping action independence.

These results show that the reason why LTCN achieves leading performance in multiple scenarios is related to the accuracy of its underlying architecture in modeling power timing characteristics. First, by introducing a dynamic contextual attention mechanism, this method can adaptively capture local changes in power disturbances in different sub-scenarios, thereby reducing response delays and false operations caused by redundant or fuzzy features. Secondly, its lightweight convolutional structure extracts multi-scale information more precisely. When dealing with multi-interference environments such as industrial areas, it can still effectively distinguish between primary and secondary disturbance signals and reduce the risk of tripping overlap. At the same time, the model maintains a high temporal and spatial resolution during the fusion of time series features, which enables it to maintain a fast and accurate response

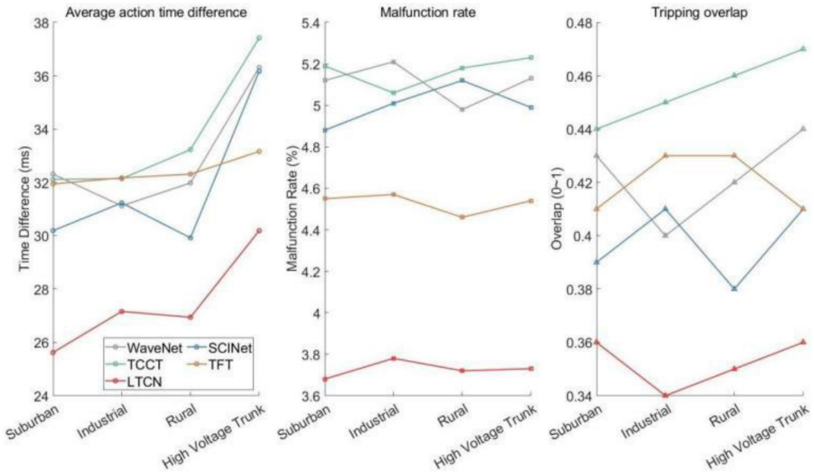


**FIGURE 4.** Comparison of protection performance indicators of different models in typical distribution scenarios

in scenarios with complex transmission characteristics such as high-voltage trunks, ensuring the stability and efficiency of the scheduling execution link. Overall, the advantage of LTCN comes from the deep adaptation of its structural optimization to the actual application scenarios of power distribution.

### OPERATION AND MAINTENANCE SCHEDULING OPTIMIZATION AND COST CONTROL CAPABILITIES

In order to quantify the cost sensitivity and economic performance of the model, this paper constructs a composite cost evaluation system of three indicators: scheduling computing cost, communication overhead and execution delay cost. Three typical operating scenarios, normal load, light load and fluctuating load, are selected to conduct a horizontal comparative analysis of the five models, WaveNet, SCINet, TCCT, TFT and LTCN. The economic evaluation covers the long-term operation and maintenance losses of the equipment, the marginal cost of model iteration and update, the indirect economic losses caused by fault misjudgment, and the impact of dynamic threshold optimization on the frequency of redundant maintenance. The results are shown in Figure 5.

The first sub-figure shows that in terms of scheduling computation cost, the LTCN model has the lowest cost under normal load, light load and fluctuating load. They are 39.1, 38.2 and 40.5 yuan per time, respectively, which is better than models such as WaveNet and TCCT. In terms of communication cost, LTCN also shows the lowest overhead, while TCCT and WaveNet have high communication costs in multiple scenarios. In the execution delay cost, the cost of LTCN under fluctuating load is 34 yuan/time, which is also at the optimal level. The delay cost of traditional models such as TFT in this scenario rises to 37.5 yuan/time, which is slightly worse.

The reasons for the above differences can be analyzed from the architecture mechanism of each model. LTCN uses a lightweight convolutional structure and a dynamic channel attention mechanism to capture multi-scale features while compressing invalid computation paths, significantly reducing scheduling computation and communication redundancy. Its dynamic gating structure also improves the ability to respond quickly to sudden load changes, so it can still maintain a low execution delay cost under fluctuating loads. In contrast, although WaveNet and TCCT have strong sequence modeling capabilities, their deep stacking structure and static computing path have high computational complexity and transmission load when facing large-scale device data scheduling, resulting in high costs. TFT has introduced a time fusion attention mechanism, and although it performs moderately under light loads, it is relatively less adaptable to data scenarios with strong volatility, which is reflected in the increase in execution costs.

**TABLE 3.** Comparison of each prediction model in terms of scheduling coverage and fault tolerance

| Model | Scheduling Coverage Rate (%) | Error Tolerance Rate (%) |
|---|---|---|
| WaveNet | 91.3 | 84.5 |
| SCINet | 92.7 | 85.1 |
| TCCT | 93.5 | 86.3 |
| TFT | 92.2 | 85.8 |
| LTCN | 96.8 | 89.7 |

In order to evaluate the global availability and fault tolerance of the model in the industrial scheduling system, this experiment conducted a comparative quantitative analysis of scheduling coverage and fault tolerance. Scheduling coverage is used to measure the ability of the model to successfully generate executable scheduling results in different task scenarios, while fault tolerance reflects the ability of the model to maintain output validity in the face of sudden disturbances or data anomalies. Table 3 shows the results of each model.

In terms of scheduling coverage, LTCN achieved 96.8%, the best performance among all models; in terms of fault tolerance, LTCN achieved 89.7%, also higher than other models. This advantage reflects the structural innovation

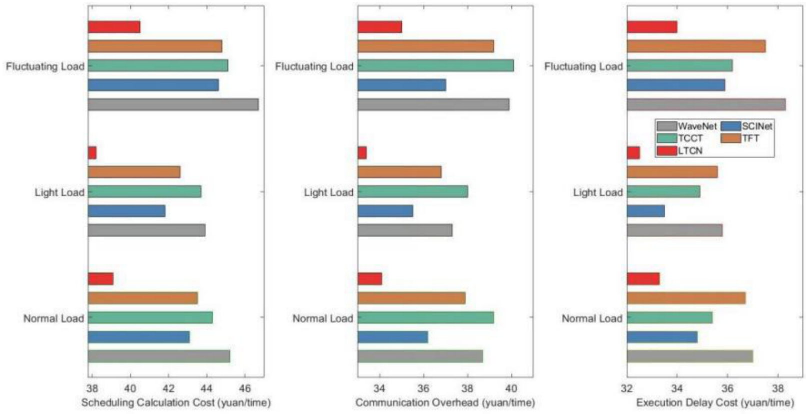


FIGURE 5. Comparison of scheduling computation cost, communication overhead and execution delay cost

and mechanism optimization of LTCN in model design. It mainly relies on lightweight temporal convolutional units and long-term dependency modeling mechanisms to improve the global coverage of scheduling tasks. In addition, LTCN has been explicitly enhanced in terms of feature robustness, which can effectively alleviate the input offset problem caused by abnormal disturbances. In comparison, models such as WaveNet are more inclined to local pattern learning, and although SCINet has improved in multi-scale modeling, it is still slightly insufficient in disturbance handling capabilities.

### *SYSTEM RESPONSE TIMELINESS AND SCHEDULING EXECUTION EFFICIENCY*

In order to evaluate the robustness and response efficiency of the scheduling model in a variable communication environment, this section quantitatively compares the average response time and its fluctuation range under five network operation scenarios. Figure 6 shows the difference in latency performance of different models under various complex working conditions.

From the results, LTCN always maintains the lowest response time in all scenarios, which is 44.0ms in the Normal Load scenario and 66.4ms in the Link Congestion scenario, and the standard deviation is controlled between 1.1-2.1, showing good stability. In contrast, other models have higher average response times and greater fluctuations, showing weaker adaptability to bandwidth bottlenecks. From the perspective of model structure, LTCN has the best response time mainly due to its lightweight local-global hybrid attention mechanism, which can reduce computational complexity while retaining key contextual features, improving processing efficiency and reducing latency. Although models such as TFT and TCCT have strong temporal modeling capabilities, they are not able to adapt to external disturbances, especially when the reasoning path is deep under sudden network fluctuations, resulting in a significant increase in response delay. SCINet and WaveNet perform relatively well in most scenarios, and their fluctuations are reasonably controlled, indicating that their hierarchical structure and residual connection mechanism are robust in alleviating the impact of scene complexity. The data in Figure 6 clearly reveals the real-time scheduling potential and algorithm bottleneck of the model in complex industrial network scenarios, providing a quantitative reference for actual deployment.

In order to evaluate the performance of the model in path selection and resource utilization, the study conducted quantitative analysis from three dimensions: the longest/shortest path hop count, corresponding delay, and path utilization. The results are shown in Table 4.

As can be seen from Table 4, the longest path of the LTCN model is only 6 hops, and the longest path delay is only 35.7 ms. In terms of short path indicators, the shortest hop number and delay of LTCN are 2 hops and 11.2 ms respectively, which further shows that its path selection has higher compactness. In terms of average path utilization, LTCN reaches 83.1%, indicating that it can more effectively improve link resource utilization in scheduling. The above performance differences are related to the scheduling strategy mechanisms of each model. Although TCCT emphasizes time-constrained transmission control, it does not explicitly compress the path length or hop count in path selection, resulting in a long path hop count. Models such as WaveNet and TFT use a certain prediction-driven mechanism to screen paths, but because they do not integrate enough spatial global structure information, path optimization has a certain locality, which is manifested as a higher hop count and suboptimal utilization. In contrast, LTCN introduces graph convolution-aware multi-scale topology encoding and combines it with a deep attention mechanism to optimize end-to-end path scheduling, which enables it to achieve better results in controlling path length, compressing transmission delay, and balancing link load.

### *EDGE NODE SYNCHRONIZATION AND COMMUNICATION THROUGHPUT PERFORMANCE*

In order to analyze the differences in network performance of the models, this section selected packet timing error, packet loss rate, and throughput, and conducted a horizontal

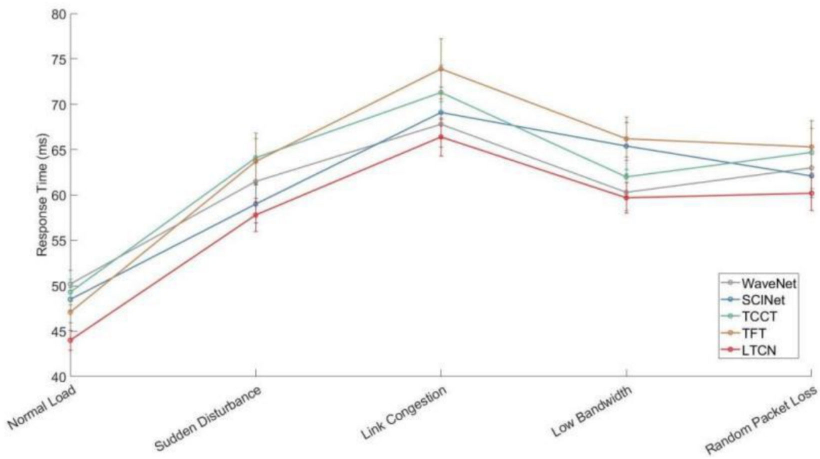


**FIGURE 6.** Comparison of response time mean and volatility of different scheduling models in multiple scenarios

**TABLE 4.** Comparison of path characteristics of each model

| Model | WaveNet | SCINet | TCCT | TFT | LTCN |
|---|---|---|---|---|---|
| Longest Path Hops | 8 | 7 | 9 | 8 | 6 |
| Shortest Path Hops | 4 | 3 | 3 | 3 | 2 |
| Longest Path Delay (ms) | 42.1 | 39.8 | 45.4 | 41.3 | 35.7 |
| Shortest Path Delay (ms) | 14.3 | 12.9 | 13.6 | 13.8 | 11.2 |
| Avg Path Utilization (%) | 76.5 | 79.2 | 74.8 | 77.0 | 83.1 |

comparison of stability and efficiency based on six sets of experimental observation data. The results are shown in Figure 7.

The first sub-graph shows that the timing error scatter points of each model under six groups of observations show obvious differences, among which the error of LTCN is concentrated in the range of 1.46ms to 2.4ms; the packet loss rate scatter points of the second sub-graph show that LTCN is between 0.36%–1.11%; the throughput indicator in the third sub-graph is in Mbps, and the LTCN value is concentrated in 74.24–78.53Mbps. These performance differences are due to the underlying design mechanisms and communication load processing strategies of each model. When deployed at the edge node, LTCN adopts an architecture based on lightweight temporal convolution combined with DCA, which can accurately capture high-frequency transient signals and implement adaptive control decisions, thereby significantly reducing the delay and loss rate of data packets on the processing link; WaveNet and TCCT have more waiting and retransmission in the computing and transmission links due to their inherent model depth and more parameter iterations, which in turn widens the timing error and packet loss fluctuation range. On the other hand, LTCN's high-speed convolutional reasoning and simplified communication protocol enable it to maintain stable throughput even under high concurrency conditions, while SCINet and TFT generate additional synchronization overhead in multi-task switching, resulting in a decline in throughput. These mechanisms together shape LTCN's comprehensive advantages in three key communication performance indicators.

### QUANTITATIVE ANALYSIS OF PROTECTION COORDINATION TIMELINESS AND RELIABILITY

To quantitatively evaluate the actual optimization effect of the Dynamic Coordination Algorithm (DCA) on the system protection performance, this section introduces the mean fault clearing time and the number of false trips/failures as core indicators. The proposed system (LTCN+DCA) is compared with two traditional methods: one is a conventional coordination strategy based on a fixed current-time curve (Conventional), and the other is a baseline system without DCA coordination, using only LTCN for fault prediction (LTCN only). Experiments were conducted in a test scenario involving multiple nested feeders, simulating 100 random short-circuit faults. The statistical results are shown in Table 5.

**TABLE 5.** Comparison of Protection Coordination Performance of Different Methods

| Performance Metrics | Conventional | LTCN only | LTCN + DCA |
|---|---|---|---|
| Mean Time to Clear Faults (ms) | 152.4 | 118.7 | 89.3 |
| Number of Malfunctions | 9 | 7 | 2 |
| Number of Refusal to Operate | 5 | 3 | 0 |
| Coordination Success Rate (%) | 86.0 | 90.0 | 98.0 |

Analysis of the data in Table 5 shows that the proposed LTCN+DCA system significantly outperforms the compara-

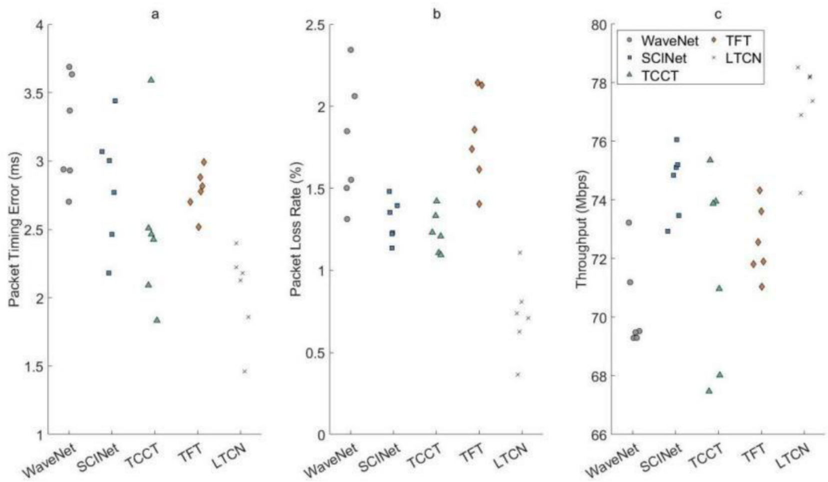


FIGURE 7. Comparison of the stability of different scheduling models under key communication performance indicators

tive methods in all key indicators. Compared to conventional coordination strategies, this system reduces the mean fault clearing time by 41.4%, directly attributable to the optimized tuning of multi-time domain thresholds by DCA, enabling protection devices to operate quickly and selectively based on real-time network conditions. Simultaneously, the system successfully suppressed false trips and failures to operate to 2 and 0 occurrences, respectively, verifying that the DCA's conflict detection and resolution mechanism effectively avoids incorrect operations caused by threshold overlap or timing interference. Ultimately, the system's coordination success rate reaches 98%, fully demonstrating its comprehensive ability to improve protection selectivity, speed, and reliability in deeply nested networks.

## VI. CONCLUSIONS

This paper constructs a real-time adaptive operation and maintenance system for drop-out fuses that integrates DCA and LTCN prediction models. Addressing the increasing grid complexity—which is acutely evident in the deeply nested networks and high-demand environments of the industry—this system solves the persistent problem of protection coordination and operation and maintenance. By collaboratively modeling the action threshold of the protection device as a mixed integer programming problem and combining it with a lightweight model, protection coordination optimization and operation and maintenance cost minimization are achieved. Experiments show that the method is superior to other models in terms of fault diagnosis accuracy, system response speed, and operation and maintenance scheduling efficiency, significantly improving the operation and maintenance efficiency of the distribution system. However, the real-time and stability of the system in large-scale complex networks still need to be further verified. In the future, the multi-agent collaboration mechanism can be expanded to enhance the robustness of the system. Furthermore, given the resource constraints and continuous operation demands typical of the industry's IIoT infrastructure, more efficient lightweight models can be explored to adapt to resource-constrained edge device scenarios.

## AUTHOR CONTRIBUTIONS

Conceptualization –Shoujun Bao, Shuhong Li, Ziyong Pan, Fuxiang Liang and, Shenghai Han; methodology – Shoujun Bao, Shuhong Li, Ziyong Pan, Fuxiang Liang and, Shenghai Han; investigation – Shoujun Bao, Shuhong Li, Ziyong Pan, Fuxiang Liang and, Shenghai Han; writing-original draft preparation – Shoujun Bao, Ziyong Pan, Fuxiang Liang and, Shenghai Han. All authors have read and agreed to the published version of the manuscript.

## CONFLICTS OF INTEREST

The authors declare no conflict of interest.

## FUNDING

This research was supported by, State Grid Qinghai Electric Power Company Science and Technology Project Funding, 522824240001, Research on Digital Monitoring and Operation of Drop type Fuses in High cold Regions Based on Beidou and Micro motion Technology.

## ACKNOWLEDGEMENTS

Not applicable.

## REFERENCES

[1] Q. Wang and M. Jing, "Multi-stage expansion planning of distribution network considering distributed power generation," Frontiers in Energy Research, vol. 10, pp. 902891-902899, 2022, doi: 10.3389/fenrg.2022.902891.

[2] P. Chen, H. Cao, X. He, Y. Yang, and L. Lin, "Distributed topology identification algorithm of distribution network based on neighboring interaction," Frontiers in Energy Research, vol. 10, pp. 910518-910527, 2023, doi: 10.3389/fenrg.2022.910518.

[3] H. Bisheh, B. Fani, G. Shahgholian, and I. Sadeghkhani, "Fuse saving coordination scheme for active distribution systems: State-of-the-art and a novel quasi-voltage current based scheme," IET Generation, Transmission & Distribution, vol. 18, no. 4, pp. 729-755, 2024, doi: 10.1049/gtd2.13110.

[4] Q. Yang, X. Rong, R. Guo, H. Zhao, and Y. Zhao, "Real-Time Detection of Insulators and Drop Fuses Based on Improved YOLOv4," Scientific Programming, vol. 2022, no. 1, pp. 5755265-5755280, 2022, doi: 10.1155/2022/5755265.

[5] A. S. T. Hussain, S. A. Ahmed, and T. A. Taha, "Early fault identification for operating circuit breaker based on classifier model system," Indonesian Journal of Electrical Engineering and Computer Science, vol. 26, no. 2, pp. 699-706, 2022, doi: 10.11591/ijeecs.v26.i2.pp699-706.

[6] M. A. Elsadd, A. F. Zobaa, H. A. Khattab, A. M. Abd El Aziz, and T. Fetouh, "Communicationless overcurrent relays coordination for active distribution network considering fault repairing periods," Energies, vol. 16, no. 23, pp. 7862-7894, 2023, doi: 10.3390/en16237862.

[7] W. Guo and Y. Shi, "A visual faulty feeder detection method for power distribution network based on spatial image generation and deep learning," IET Generation, Transmission & Distribution, vol. 17, no. 24, pp. 5430-5445, 2023, doi: 10.1049/gtd2.13055.

[8] N. M. Rodrigues, F. M. Janeiro, and P. M. Ramos, "Power quality transient detection and characterization using deep learning techniques," Energies, vol. 16, no. 4, pp. 1915-1926, 2023, doi: 10.3390/en16041915.

[9] C. Lothongkam, T. Patcharoen, and S. Yoomak, "Effect of the drop out fuse connection scheme on the overvoltage and the surge arrester in a distribution system," Energy Reports, vol. 9, pp. 41-47, 2023, doi: 10.1016/j.egyr.2023.08.058.

[10] Y. Zuo, Z. Xu, and R. Jiang, "Analysis and thinking on a fault caused by the expansion and cracking of the porcelain insulation support of a drop-out fuse," Rural Electrification, vol. (12), pp. 22-24, 2022, doi: 10.13882/j.cnki.ncdqh.2022.12.005.

[11] E. N. Odonkor, A. K. Awopone, and P. N. Ayambire, "Design of an Intelligent Monitoring System for Distribution Transformer Protection Systems for Rural Communities," International Journal of Applied, vol. 12, no. 1, pp. 22-35, 2022, doi: 10.30845/ijast.v12n1p3.

[12] X. Jing, Z. Wu, L. Zhang, Z. Li, and D. Mu, "Electrical fault diagnosis from text data: A supervised sentence embedding combined with imbalanced classification," IEEE Transactions on Industrial Electronics, vol. 71, no. 3, pp. 3064-3073, 2023, doi: 10.1109/TIE.2023.3269463.

[13] X. Liu, "Practical exploration and application analysis of distribution network operation and maintenance," Hydropower Technology, vol. 6, no. 3, pp. 117-119, 2023, doi: 10.33142/hst.v6i3.8548.

[14] H. Xu, "Fault analysis and troubleshooting examples of distribution transformers," Rural Electrification, vol. (4), pp. 50-56, 2025, doi: 10.13882/j.cnki.ncdqh.2502A027.

[15] S. Li, B. Miao, D. Zhang, X. Zhou, Z. Lin, and X. Guo, "Analysis of fuse overload breaking test system and test method," Electrical Appliances and Energy Efficiency Management Technology, vol. (10), pp. 70-76, 2023, doi: 10.16628/j.cnki.2095-8188.2023.10.011.

[16] J. Zheng, G. Wang, B. Lin, C. Liu, X. Liu, and C. Zang, "Experimental study on the small current fusing characteristics of medium voltage transformer protection fuses," Electrical Appliances and Energy Efficiency Management Technology, vol. (7), pp. 1-7, 2022, doi: 10.16628/j.cnki.2095-8188.2022.07.001.

[17] M. Ayalew, B. Khan, and Z. M. Alaas, "Optimal service restoration scheme for radial distribution network using teaching learning based optimization," Energies, vol. 15, no. 7, pp. 2505-2525, 2022, doi: 10.3390/en15072505.

[18] A. Azizi, B. Vahidi, and A. F. Nematollahi, "Reconfiguration of active distribution networks equipped with soft open points considering protection constraints," Journal of Modern Power Systems and Clean Energy, vol. 11, no. 1, pp. 212-222, 2023, doi: 10.35833/MPCE.2022.000425.

[19] A. Filba-Martinez, S. Busquets-Monge, S. Alepuz, et al., "An intelligent electronic fuse for selective isolation of faulty switching cells in power electronic converter legs to guarantee continuous operation," IEEE Journal of Emerging and Selected Topics in Power Electronics, vol. 10, no. 6, pp. 7665-7676, 2022, doi: 10.1109/JESTPE.2022.3183160.

[20] J. Zhu, W. Gao, Y. Li, X. Guo, G. Zhang, and W. Sun, "Power System State Estimation Based on Fusion of PMU and SCADA Data," Energies, vol. 17, no. 11, pp. 2609-2628, 2024, doi: 10.3390/en17112609.

[21] G. Wang, "Research on fault diagnosis and intelligent maintenance technology of power grid equipment," Hydropower Technology, vol. 8, no. 11, pp. 73-76, 2025, doi: 10.33142/hst.v8i11.18304.

[22] J. Łukasiak, M. Wiśnios, and A. Rosiński, "Method for Evaluating the Effectiveness of Electrical Circuit Protection with Miniature Fuse-Links," Energies, vol. 16, no. 2, pp. 960-988, 2023, doi: 10.3390/en16020960.

[23] N. Shao, Q. Chen, C. Yu, D. Xie, and Y. Sun, "Fault Tracing Method for Relay Protection System–Circuit Breaker Based on Improved Random Forest," Electronics, vol. 13, no. 3, pp. 582-619, 2024, doi: 10.3390/electronics13030582.

[24] A. Ağın, A. Demirören, and Ö. Usta, "A novel approach for power system protection simulation via the iec 61850 protocol," IEEE Access, vol. 12, pp. 107656-107669, 2024, doi: 10.1109/ACCESS.2024.3436572.